Chemical Science

EDGE ARTICLE

View Article Online
View Journal | View Issue

Cite this: *Chem. Sci.*, 2015, **6**, 4131

Solid-phase synthesis provides a modular, lysine-based platform for fluorescent discrimination of nitroxyl and biological thiols†

Andrei Loas, Robert J. Radford, Alexandria Deliz Liang and Stephen J. Lippard*

We describe a modular, synthetically facile solid-phase approach aimed at separating the fluorescent reporter and binding unit of small-molecule metal-based sensors. The first representatives contain a lysine backbone functionalized with a tetramethylrhodamine fluorophore, and they operate by modulating the oxidation state of a copper ion ligated to an [N_4] (cyclam) or an [N_2O] (quinoline-phenolate) moiety. We demonstrate the selectivity of their Cu(II) complexes for sensing nitroxyl (HNO) and thiols (RSH), respectively, and investigate the mechanism responsible for the observed reactivity in each case. The two lysine conjugates are cell permeable in the active, Cu(II)-bound forms and retain their analyte selectivity intracellularly, even in the presence of interfering species such as nitric oxide, nitrosothiols, and hydrogen sulfide. Moreover, we apply the new probes to discriminate between distinct levels of intracellular HNO and RSH generated upon stimulation of live HeLa cells with ascorbate and hydrogen sulfide, respectively. The successful implementation of the lysine-based sensors to gain insight into biosynthetic pathways validates the method as a versatile tool for producing libraries of analogues with minimal synthetic effort.

Received 10th March 2015
Accepted 5th May 2015

DOI: 10.1039/c5sc00880h

www.rsc.org/chemicalscience

Introduction

The discovery of nitric oxide (NO) as the endothelium-derived relaxing factor[1] sparked great scientific interest in this small gaseous biological regulator. A diatomic radical, NO functions as a signaling agent for a variety of processes related to the cardiovascular and immune systems,[2] neuroprotection,[3] protein regulation[4] and chemotherapeutic resistance.[5] In contrast, nitroxyl (HNO), the protonated, one-electron reduced form of nitric oxide, has attracted considerably less attention.[6,7] Even though enzymatic production of HNO remains an unanswered question, several biosynthetic pathways leading to its endogenous generation have been investigated.[8–11] HNO was recently detected intracellularly in the reaction between HSNO and H_2S,[12] in the heme-catalyzed reduction of nitrite,[13] and in the decomposition of *O*-nitrosoascorbate.[14] Exogenously applied HNO displays a significantly different biochemistry from that of NO, leading to, among others, vasoprotective effects,[15] heart muscle contractility,[16] and neurotoxicity.[17] As NO and HNO display contrasting biological roles, molecular reporters able to discriminate between the two species are highly desirable. At the same time, the probes should maintain selectivity for NO or HNO in the presence of other reactive nitrogen and oxygen species (RNOS) and biological reductants such as ascorbate, hydrogen sulfide, and thiols. The reactivity of NO and HNO presents a challenge in the design of sensors suitable for investigating their generation and biological functions.[18] In this respect, fluorescence microscopy with small-molecule probes has emerged as the preferred biologically non-intrusive method.[19]

Within the broad field of fluorescent sensors, transition metal-based complexes offer a practical solution for direct and selective detection of the desired analyte. In the past decade, our group has developed several families of sensors for nitric oxide,[20–26] employing a Cu(II) ion coordinated to the tridentate [N_2O] motif of a quinoline-phenolate binding site, as in the parent, fluorescein-based CuFL1 (Fig. 1).[21]

In its resting state, emission of the fluorescein fluorophore in CuFL1 is quenched by the paramagnetic Cu(II) ion. Upon reaction with NO, deprotonation and nitrosation of the amine occurs with concomitant dissociation of the metal ion from the complex as a reduced Cu(I) species, and fluorescence emission is restored in the resulting nitrosamine product.[20,21,29] On the other hand, fluorescent Cu(II)-based probes for nitroxyl operate solely through a copper reduction mechanism.[30] To ensure selectivity in biological milieu, sensors for nitroxyl should ideally have a Cu(II/I) reduction potential tuned between that of NO (−0.68 V *vs.* NHE at pH 7)[31] and cysteine (−0.36 V *vs.* NHE at

Department of Chemistry, Massachusetts Institute of Technology, 77 Massachusetts Avenue, Cambridge, MA 02139, USA. E-mail: lippard@mit.edu; Fax: +1-617-258-8150; Tel: +1-617-253-1892

† Electronic supplementary information (ESI) available: Experimental procedures, reaction schemes, NMR and MS spectra, HPLC traces, additional fluorescence emission spectra, selectivity of CuQLF, determination of Cu(II) dissociation constants, cyclic voltammetry studies, simulated EPR spectra, full-field view fluorescence microscopy images. See DOI: 10.1039/c5sc00880h

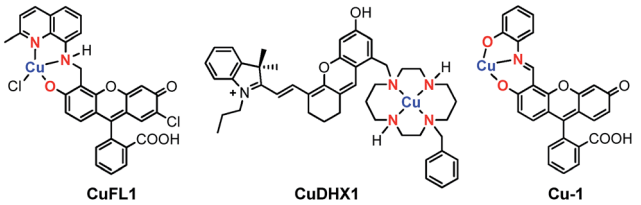

Fig. 1 Structures of Cu(II)-based small-molecule fluorescent probes selective for NO (CuFL1),[21] HNO (CuDHX1),[27] and cysteine (**Cu-1**),[28] highlighting in red the ligating atoms at the metal-binding sites.

pH 7).[32] In this regard, cyclam is an excellent choice for the metal-binding group in HNO sensors, owing to its tight binding of Cu(II) ($pK_d \approx 25$)[33] and the slow reaction of Cu–cyclam complexes with H_2S and thiols.[34] These criteria are validated in CuDHX1, the first near-infrared-emitting probe for HNO (Fig. 1).[27] Metal-free fluorescent probes for HNO have also been developed based on its reaction with triphenylphosphines.[35,36] In contrast to HNO probes, recently reported Cu-based fluorescent sensors for H_2S and thiols rely on the affinity of Cu(II) for the sulfide or thiolate anions, respectively.[37–40] For example, addition of cysteine to the Cu(II)–iminofluorescein complex **Cu-1** (Fig. 1) leads to decomplexation of the metal and hydrolysis of the imine to form the brightly fluorescent fluorescein aldehyde.[28] Achieving selectivity for thiols over H_2S in metal-based probes remains a rare event, however.[39,40] The different foregoing mechanisms highlight the importance of the proton- and metal-binding properties of the fluorescent ligand in imparting selectivity for a particular analyte.

Small-molecule fluorescent probes are typically obtained through cumbersome procedures involving several purification steps. New methods to facilitate sensor production and derivatization while circumventing complex syntheses are therefore highly desirable. In addressing this objective, we departed from traditional preparative routes. Making use of the unmatched ease and versatility offered by solid-phase synthesis, we introduce in this study a modular approach directed at separating the fluorophore and metal-chelating units of amino acid-based sensing constructs. We apply this method to generate the first analogues containing a single lysine (Lys) linker and further investigate the mechanism by which their Cu(II) complexes acquire selectivity for a particular bioanalyte. Finally, we demonstrate the utility and biological compatibility of the new probes through their ability to detect changes in intracellular nitroxyl and thiol concentrations *in vitro*.

Results and discussion

Design, synthesis, and photophysical properties

We prepared the new lysine-based fluorescent probes according to the synthetic strategy depicted in Scheme 1.

Starting from a Rink amide resin, an orthogonally and doubly protected PG2-Lys(PG1)-OH linker was introduced on the solid-phase support. Deprotection of the PG1 group at the Lys ε-position afforded a free amine, which was then coupled under standard conditions (see ESI†) with a carboxy-

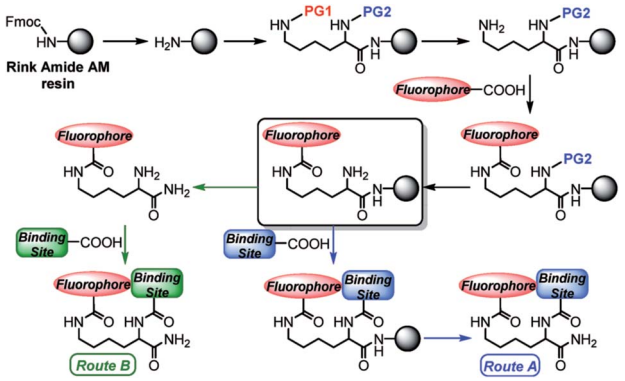

Scheme 1 General solid-phase strategy for production of fluorescent lysine-based sensing constructs. Abbreviations: Fmoc = fluorenylmethyloxycarbonyl; PG1, PG2 = orthogonal amine-protecting groups.

functionalized fluorophore. After a second deprotection of the N-terminal PG2 group, the metal-binding site could be added directly on the resin. The final construct was cleaved with trifluoroacetic acid (TFA) (Route A, Scheme 1). Alternatively, for binding sites labile to the strongly acidic conditions of the TFA treatment, the construct containing the free N-terminal amine was first cleaved from the resin, and the final coupling reaction was performed in solution (Route B, Scheme 1). Notably, in order to obtain metal-free ligands, a single purification step is needed for Route A, whereas two purifications are required for Route B. Even though the final constructs obtained in this work contain C-terminal amide groups on the Lys backbone, the approach described herein is applicable to a wide range of commercially available resins, including those affording C-terminal free acid residues, or for which milder cleavage conditions can be used to address the chemical stability of the intermediates.

Building on knowledge gained from designing CuDHX1,[27] we sought to achieve HNO selectivity for the first lysine conjugate, produced by employing Fmoc-Lys(Mtt)-OH as the linker, the yellow-emitting ($\lambda_{em} \approx 580$ nm) rhodamine scaffold as the fluorescent moiety, and cyclam as the metal-binding site. Isomerically pure 5-carboxytetramethylrhodamine (5-CO_2H-TAMRA, Scheme S3†)[41] was first coupled to the Lys ε-position. Following reaction with iodoacetic acid *N*-hydroxysuccinimide ester (**S9**, Scheme S3†),[42] the binding site was appended by stirring the resin with excess cyclam overnight in a dichloromethane–methanol solution. Cleavage and purification of the construct by semi-preparative HPLC afforded the cyclam–Lys–TAMRA conjugate (CLT, Fig. 2) in 21% yield based on the resin loading.

The Cu(II) complexes of NO[20–24] and HNO[27,30] metal-based sensors are typically generated *in situ* immediately before use by adding equimolar amounts of $CuCl_2$ to concentrated stock solutions of the fluorescent ligands. Coordination of Cu(II) by the cyclam site of CLT in a 1 : 1 ratio was achieved over several hours (data not shown). We wanted to avoid the long waiting time required to prepare the complex *in situ*, and anticipated that the high affinity of cyclam for Cu(II)[33] might allow for pre-

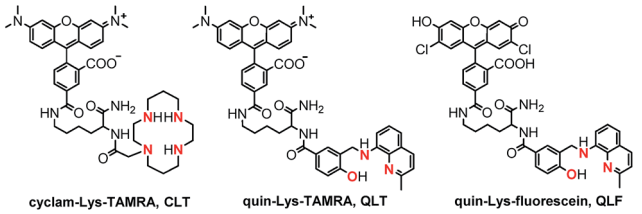

Fig. 2 Structures of the three fluorescent lysine conjugates obtained through the solid-phase approach of Scheme 1, highlighting in red the ligating atoms of the metal-binding sites. See ESI and Schemes S2–S5† for synthetic intermediates and experimental procedures.

formed CuCLT to withstand chromatographic separations and subsequent storage either in the solid state or as stock solutions. Indeed, mixing pure CLT overnight with excess $CuCl_2$ in water afforded CuCLT (Scheme S3†), which was purified by HPLC and isolated as its TFA salt in 61% yield.

Taking note of the $[N_2O]$ metal-binding motif of NO-selective CuFL sensors (Fig. 1), we next directed our synthetic efforts toward producing a second lysine construct in which the cyclam of CLT was replaced with a quinoline-phenolate moiety, retaining the TAMRA fluorescent unit. To achieve this goal, a benzoic acid precursor containing the binding motif (**S8**, Scheme S2†) was prepared in a sequence involving reductive amination of 8-aminoquinaldine with methyl 4-formyl-3-hydroxybenzoate, followed by hydrolysis of the methyl benzoate intermediate (**S7**, Scheme S2†). Initial attempts at coupling **S8** directly on the resin (Route A, Scheme 1) resulted in de-benzylation of the desired product during cleavage with TFA (data not shown). We avoided acid-induced labilization of the quinoline-phenolate moiety by performing the reaction of **S8** with the free N-terminal amine of Lys–TAMRA in solution (Route B, Scheme 1). In a simplified procedure using Boc-Lys(Fmoc)-OH instead of Fmoc-Lys(Mtt)-OH, H-Lys–TAMRA (**S10**, Scheme S4, ESI†) was obtained in 24% isolated yield. The final quin–Lys–TAMRA conjugate (QLT, Fig. 2) was produced through amide coupling of H-Lys–TAMRA with **S8** (Scheme S4, ESI†), and was isolated in 17% yield.

In order to test the generality while retaining modularity of the solid-phase approach described in Scheme 1, we replaced the TAMRA fluorophore of QLT with a green-emitting dichlorofluorescein scaffold. Using Boc-Lys(Fmoc)-OH and 3′,6′-diacetyl-2′,7′-dichloro-5-carboxyfluorescein (5-CO_2H-FL, Scheme S5†),[43] H-Lys–fluorescein (**S11**, Scheme S5†) was synthesized in a similar manner to H-Lys–TAMRA, albeit in a low, 6% isolated yield. Following the coupling of H-Lys–fluorescein with **S8** under standard conditions in solution, the quin–Lys–fluorescein conjugate (QLF, Fig. 2) was obtained in 17% yield.

The identity and purity of CLT, CuCLT, QLT, and QLF were confirmed by spectroscopic and chromatographic techniques (see ESI and Fig. S1–S15†). The photophysical parameters of the three lysine conjugates were determined in aqueous buffer, pH 7.0 (Table S1, ESI†). In the metal-free form, CLT and QLT display absorption bands with maxima at 552 and 556 nm, respectively. QLF, on the other hand, absorbs at 511 nm. No spectral shifts were observed in the visible spectrum upon binding of Cu(II) to any of the three constructs, and only minor changes occurred in their molar absorptivities. Both the metal-free and Cu(II)-bound forms of CLT and QLT emit in the yellow spectral region at ~580 nm (Table S1†). The analogous species of QLF exhibit green fluorescence maxima centered at ~530 nm. The average brightness ($\varepsilon \times \Phi$) values of the CLT, QLT, and QLF constructs were determined to be 3.71×10^4, 5.41×10^3, and 2.33×10^3 M^{-1} cm^{-1}, respectively.

Analyte selectivity

With CuCLT in hand, its reactivity toward HNO was first investigated. Addition of excess HNO donor Angeli's salt[44,45] to buffered aqueous solutions of CuCLT under anaerobic conditions resulted in an immediate ~4-fold increase in fluorescence emission (Fig. 3A), thus confirming that the separation of the cyclam binding site from the fluorophore in the CLT ligand retains the HNO-sensing ability of the construct. A time-resolved fluorescence spectroscopy study revealed that the maximum emission turn-on of CuCLT upon reaction with HNO occurs ~5 min after addition of Angeli's salt (Fig. S18A†). The dynamic range of the probe is in line with values previously reported for other Cu(II)-based HNO sensors,[26,27,30] but remains significantly lower by comparison with reaction-based analogs.[35,36]

We also determined ~0.4 equiv. to be the lowest amount of Angeli's salt required to induce a ≥10% increase in the integrated emission of 5 μM CuCLT at pH 7 (Fig. 3B). Remarkably, the sensitivity of CuCLT toward HNO was more than 100-fold greater than the CuDHX1 sensor containing a similar cyclam metal-binding site (*i.e.*, 50 equiv. Angeli's salt).[27] The detection limit (see ESI†) of CuCLT for Angeli's salt calculated under these conditions is 360 nM. Because of the difficulties in estimating the exact concentration of HNO in an aqueous solution of Angeli's salt and the marked reactivity of nitroxyl,[45] we refrain from reporting a detection limit of CuCLT for HNO.

The NO reactivity of CuQLT and CuQLF was investigated next. Addition of excess NO gas or the NO donors *S*-nitroso-*N*-acetyl-DL-penicillamine (SNAP) and *S*-nitrosoglutathione (GSNO) to air-free aqueous solutions of the probes did not elicit a fluorescence response at pH 7. Instead, CuQLT and CuQLF

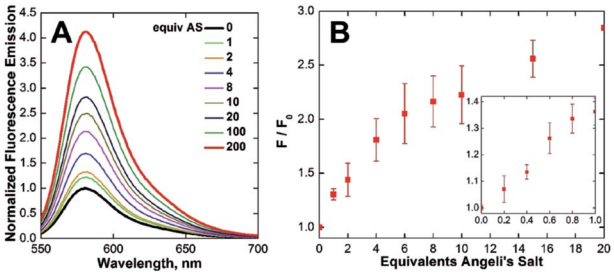

Fig. 3 Normalized (A) fluorescence emission spectra and (B) integrated fluorescence response of 3.3 μM CuCLT *vs.* added Angeli's salt (AS) in aqueous buffer under anaerobic conditions (25 °C, 100 mM KCl, 50 mM PIPES, pH 7.0, $\lambda_{ex} = 540$ nm). The inset shows the response of 5 μM CuCLT in the sub-stoichiometric range, recorded separately under similar conditions.

displayed 5.5- and 10-fold increases in their integrated fluorescence emission following treatment with excess L-cysteine (Cys) (Fig. 4, 5, and S20†), suggesting that the two complexes might be useful as sensors for biological thiols.

Time-dependent fluorescence spectroscopy indicated that the reaction of CuQLT with Cys was complete after ~25 min (Fig. S18B†). Furthermore, the lowest amount of Cys required to induce a ≥10% increase in the integrated emission of 1 μM CuQLT at pH 7 was determined to be ~4 equiv. (Fig. 4B), corresponding to a detection limit of 1.2 μM. The inertness of CuQLT and CuQLF toward NO demonstrates how separation of the binding motif from the fluorophore can lead to unexpected chemistry in the final sensing construct.

We evaluated the ability of CuCLT, CuQLT, and CuQLF to selectively detect nitroxyl and thiols, respectively. A thorough study of the fluorescence response of the three probes was conducted against a broad range of RNOS and other species present in live cells (Fig. 5 and S20†). In pH 7 buffered aqueous solutions, CuCLT remained selective for nitroxyl over any other analyte that we investigated, including reducing agents such as H_2S, ascorbate, and thiols. On the other hand, CuQLT was selective for cysteine and glutathione over all other species studied except nitroxyl, which generated a minor ~2-fold fluorescence increase (Fig. 5). A strong fluorescence increase occurred when CuQLT was treated with SNAP and GSNO in air (Fig. 5), consistent with the accelerated aerobic decomposition of the NO donors in the presence of copper ions[46] and concomitant formation of the corresponding thiols. Notably, the selectivity for thiols was retained when the tetramethylrhodamine fluorophore of CuQLT was replaced with dichlorofluorescein in CuQLF (Fig. S20†). Addition of Cys to aqueous solutions of the metal-free QLT and QLF ligands did not produce a change in fluorescence emission (Fig. S17†), confirming that binding of Cu(II) is required in order to impart reactivity toward thiols. Given that Cu(II)-based sensors are typically susceptible to HS^-/S^{2-} attacks,[39,40] the selectivity of the three sensors for nitroxyl and thiols over hydrogen sulfide is of particular importance in view of their potential applications in a biological system. To further test their inertness toward sulfide, aqueous solutions of the sensors were saturated by H_2S gas, revealing no increase in fluorescence emission in either case (Fig. S16†). The results of the selectivity study recommend CuCLT, CuQLT, and CuQLF as suitable sensors for use in biological samples without interference from H_2S and NO-generating species.

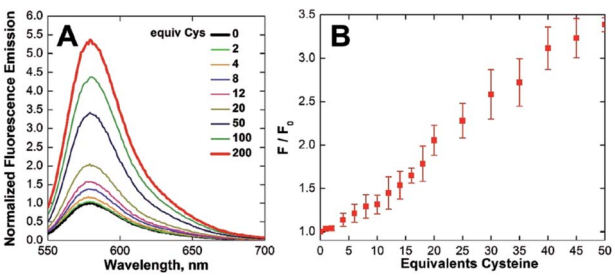

Fig. 4 Normalized (A) fluorescence emission spectra and (B) integrated fluorescence response of 1 μM CuQLT *vs.* added L-cysteine (Cys) in aqueous buffer (25 °C, 100 mM KCl, 50 mM PIPES, pH 7.0, λ_{ex} = 540 nm).

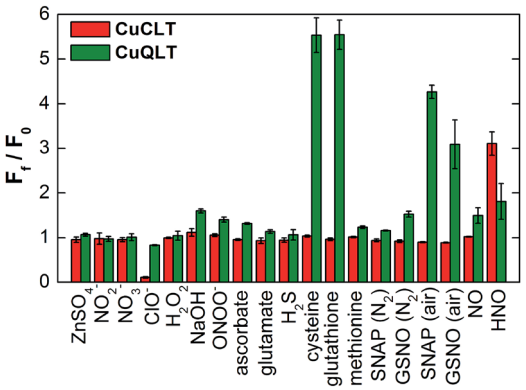

Fig. 5 Selectivity of 2 μM CuCLT and CuQLT toward RNOS and other biological analytes in aqueous buffer (37 °C, 100 mM KCl, 50 mM PIPES, pH 7.0). For each sample, the fluorescence emission was recorded in triplicate before and 20 min after addition of excess analyte (1500 equiv. NO, 500 equiv. all other). The measurements for OH^- were conducted in 10 mM aq. NaOH. The integrated fluorescence response was normalized in each case to the initial fluorescence of the metal-bound complexes. In all cases, excitation was provided at 540 nm and the emission intensity was integrated between 550 and 700 nm.

Mechanistic investigations

Having established the reactivity of the three lysine-based probes in the cuvette, we next attempted to elucidate the mechanisms responsible for the observed chemistry.

Cu(II) dissociation constants. The Cu(II)-binding properties of QLT and QLF were first investigated. When $CuCl_2$ was titrated into 5 μM aqueous solutions of the ligands at pH 7, small spectral changes occurred in the UV-vis absorption spectra of the tetramethylrhodamine and dichlorofluorescein fluorophores, respectively. By fitting the absorbance changes to a one-step binding equation,[21] we obtained Cu(II) dissociation constants ($K_{d,Cu}$) of 3.3 ± 0.8 and 15.0 ± 2.8 μM for QLT and QLF, respectively (Fig. S19A and B†). The value for CuQLT is comparable to that of CuFL1 ($K_{d,Cu}$ = 1.5 ± 0.3 μM).[20] The ~5-fold decrease in the affinity of QLF for Cu(II) with respect to QLT may be explained by steric and electronic interference of the phenolate group of the dichlorofluorescein chromophore in the binding process. The methyl benzoate ester precursor of QLT and QLF (**S7**, Scheme S2†) had a $K_{d,Cu}$ an order of magnitude higher (0.13 ± 0.03 μM, Fig. S19C†).

Cyclic voltammetry. The Cu(II)/Cu(I) reduction potentials of CuCLT and CuQLT were measured with a three electrode setup in quiescent, nitrogen sparged acetonitrile solutions. In order to facilitate the assignment of the Cu-centered events for each sensor, cyclic voltammograms of the CLT and QLT ligands were also recorded. Both metal-free ligands exhibited characteristic rhodamine-centered[47] one-electron reductions at −1.27 and −1.15 V *vs.* Fc/Fc^+, respectively (Fig. S21†). In acetonitrile, CuCLT displayed an irreversible Cu(II)/Cu(I) reduction at −1.06

V *vs.* the Fc/Fc^+ internal standard (Fig. S22A†). The reduction of NO to NO^- in acetonitrile occurs at −1.42 V *vs.* Fc/Fc^+,[31] and therefore nitroxyl should be able to reduce Cu(II) in CuCLT. We also measured the reduction potential of CuCLT in phosphate-buffered saline (PBS, pH 7.4). Using a Ag/AgCl reference electrode, we observed a quasireversible Cu(II)/Cu(I) reduction centered at −0.8 V *vs.* NHE (Fig. S23†). The irreversible reduction and protonation of NO to form HNO at pH 7 is estimated to occur at potentials ranging from −0.8 to −0.5 V *vs.* NHE,[7,14,31,48,49] but the thermodynamic potential of the NO, H^+/HNO couple is not known. The reduction potentials of cysteine, glutathione and H_2S are significantly more positive at pH 7 (−0.36, −0.29, and −0.24 V *vs.* NHE, respectively),[32] and therefore neither should be able to thermodynamically reduce CuCLT. These observations are consistent with the fluorescence turn-on of CuCLT only in the presence of HNO. In the case of CuQLT prepared *in situ*, a quasireversible Cu(II)/Cu(I) reduction was observed at 0.19 V *vs.* Fc/Fc^+ (Fig. S22B†). Even though the positive $E_{1/2}$ value supports the reduction of the metal center in CuQLT by thiols, it does not account for the lack of fluorescence response observed upon addition of HNO or H_2S. Consequently, the selectivity for thiols displayed by CuQLT cannot be explained on thermodynamic grounds alone.

EPR and NMR spectroscopy. X-band electron paramagnetic resonance (EPR) spectra of CuCLT and CuQLT were measured at 77 K in methanol, in the absence and after addition of 100 equiv. of Angeli's salt and cysteine, respectively. The initial spectrum obtained for CuCLT (Fig. 6A) showed a rhombic Cu(II) signal with $g_{xyz} = 2.195$, 2.055, and 2.027. A similar signal ($g_{xyz} =$ 2.195, 2.048, and 2.027) was observed 5 min after anaerobic treatment with excess Angeli's salt. Simulation of both EPR spectra was performed in order to obtain the principal g values (Fig. S24A and B†).

The small change observed only for the g_y component upon addition of Angeli's salt ($\Delta g_y = 0.007$) calls into question a conclusion based on EPR data regarding changes in the metal coordination environment. The inability to trap the reduced Cu(I) form upon reaction with nitroxyl was previously reported for cyclam-based HNO sensors.[27] This result suggests that reduction of Cu(II) to Cu(I) by HNO is followed by a fast re-oxidation of the Cu(I) species by residual oxygen admitted to the EPR tube, by NO produced in the reaction of HNO with CuCLT, or by one of the degradation products of HNO in solution.[45] Cu(I)-mediated disproportionation of NO is a well-documented transformation leading to Cu(II)–NO_2^- and N_2O.[50] Proton-assisted reduction of NO with Cu(I) complexes was previously reported.[51] Furthermore, the reduction potential of −0.8 V *vs.* NHE determined for CuCLT in PBS shows that it can be oxidized by NO. The fluorescence turn-on observed upon addition of Angeli's salt to CuCLT in methanol confirmed that a reaction with HNO took place (Fig. S26A†). An ESI-MS analysis of the EPR solutions of CuCLT with and without added Angeli's salt (Fig. S25†) revealed for the former a species with $m/z = 906.5$, consistent with an $[M + NO_2]^+$ formula in which the trifluoroacetate counterions are replaced with nitrite anions, which can accumulate in solution as a result of decomposition of Angeli's salt[45] or disproportionation of NO.[50,51] Treatment of CuCLT with 100 equiv. of $NaNO_2$ in methanol did not produce a fluorescence turn-on (Fig. S26B†), confirming that HNO is the species responsible for the observed reactivity. Furthermore, the CuCLT + $NaNO_2$ solution displayed an EPR signal identical to the initial spectrum of CuCLT recorded in the absence of Angeli's salt (Fig. S24D†).

Taken together, the foregoing data support reduction of Cu(II) in CuCLT by HNO followed by a fast reoxidation with retention of copper in the cyclam binding site. This hypothesis is further confirmed by the broad resonances and small (<0.1 ppm) differences in chemical shifts observed in the ^1H NMR spectra of CuCLT acquired before and after anaerobic addition of Angeli's salt (Fig. S27†).

In the case of CuQLT, the EPR spectrum recorded in the absence of cysteine showed an axial signal with $g_{\|} = 2.415$ and $g_{\perp} = 2.079$ (Fig. 6B); the simulated trace is provided in Fig. S24C.† The signal may be assigned to a distorted tetrahedral Cu(II) complex, consistent with coordination of the $[N_2O]$ binding site and an additional ligand, possibly Cl^- originating from the $CuCl_2$ stock solution used to prepare the complex *in situ*. Upon anaerobic addition of 100 equiv. of cysteine, the solution became EPR-silent, indicating reduction to Cu(I). ESI-MS of this solution revealed the peak of the protonated QLT ligand at $m/z = 848.5$ as the only detectable species (Fig. S25D†). The silent EPR signal was preserved upon exposure of the CuQLT + Cys solution to air for 15 min (Fig. 6B). We note that stable Cu(I)–Cys complexes were previously isolated under anaerobic conditions.[52] In a ^1H NMR spectroscopic study, broadening of the QLT resonances was observed after addition of $CuCl_2$ to the NMR tube, confirming that binding of Cu(II) had occurred (Fig. S28†). Subsequent addition of excess Cys to the

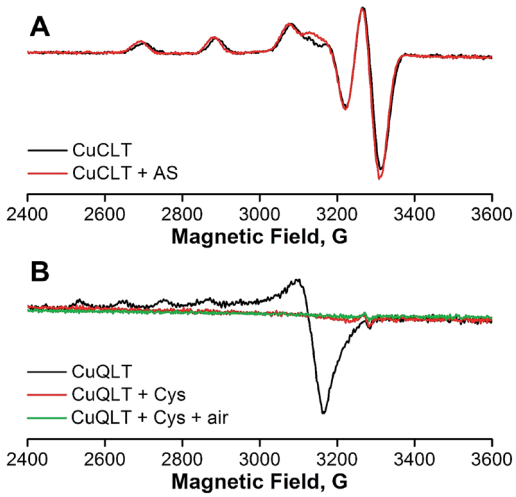

Fig. 6 X-band EPR spectra of anaerobic 400 μM solutions of (A) CuCLT and (B) CuQLT in methanol, recorded in the absence (black lines) and after the addition (red lines) of 100 equiv. of (A) Angeli's salt and (B) L-cysteine, respectively. The solutions were removed from the glove box and frozen 5 and 15 min after the addition of the analytes, respectively. Collection parameters: temperature, 77 K; modulation amplitude, 20 G; microwave power, 0.02 mW at 9.16 GHz.

same sample sharpened the ^{1}H resonances, in support of the EPR results indicating Cu(II) reduction. Even though metal decomplexation has been documented as the mechanism responsible for thiol sensing in previously reported Cu(II)-based fluorescent probes,[28,53,54] EPR studies, to the best of our knowledge, have not yet been performed to address the oxidation state and stability of the derived Cu species. In conclusion, the spectroscopic observations for CuQLT favor metal reduction by thiolates and removal of the Cu(I) ion from the quinoline-phenolate binding site together with enhancement of fluorescence emission.

Live cell imaging studies

The ability of the new probes to detect their specific analytes *in vitro* was investigated in live HeLa cells. Both TAMRA-based lysine conjugates CuCLT and CuQLT readily enter cells following incubation at concentrations of 3 to 5 μM. Because of its chemical inertness to thiols, CuCLT was incubated in either PBS or dye- and serum-free DMEM growth medium. Incubation of cells with CuQLT was performed exclusively in PBS to avoid interference of thiols. The fluorescein-based construct CuQLF displayed insufficient cellular permeability for detection of a fluorescent signal, therefore preventing its application as an intracellular probe for biological thiols (Fig. S30†).

Cytotoxicity of CuCLT. Cytotoxic sensors cannot be used for biological imaging. We therefore assessed the cytotoxicity of CuCLT by the MTT assay in HeLa cells. Data recorded 24 h after treatment with concentrations of CuCLT up to 5 μM (Fig. S29†) indicated that CuCLT is essentially nontoxic and can be applied in biological studies requiring lengthy incubation times. The cytotoxicity of the thiol-selective probe CuQLT precluded its evaluation by the MTT assay, for reasons mentioned above.

Intracellular detection of HNO with CuCLT. Addition of exogenous Angeli's salt to HeLa cells incubated with CuCLT displayed an immediate ~1.5-fold turn-on in the integrated intracellular fluorescence of the sensor (Fig. 7A–C). On the other hand, exogenous Na_2S did not increase the fluorescence signal (Fig. 7D–F), demonstrating that CuCLT can be successfully used to selectively detect HNO over H_2S in biological milieu. The relatively rapid (within 5 min) intracellular turn-on of CuCLT with HNO closely matches the kinetics observed in the cuvette (Fig. S18A†), although with a substantially lower dynamic range.

Co-localization analysis of CuCLT with various organelle markers revealed a moderate[55] correlation in overlap with LysoTracker Green (Pearson's correlation coefficient,[56] $r = 0.5 \pm 0.1$, $N = 34$, Fig. 8), suggesting preferential, but not exclusive accumulation of the sensor in acidic vesicles. To confirm that the partially punctate pattern observed is not due to attachment of CuCLT to the outer cellular membrane, we assembled 3D representations of the cells from images collected along the *Z*-axis. The spatial distribution of CuCLT, determined from the reconstructed 3D overlays of CuCLT and the nuclear stain Hoechst 33258 (Fig. S32†), clearly indicates internalization of the sensor inside the cells.

Co-incubation of HeLa cells with CuCLT and the NO-selective probe Cu_2FL2E,[23] and the subsequent addition of excess NO donor GSNO, generated a strong, ~3.6-fold increase only in the intracellular green fluorescence emission of Cu_2FL2E, demonstrating that CuCLT retains selectivity for HNO over NO and *S*-nitrosothiols in cells (Fig. 9).

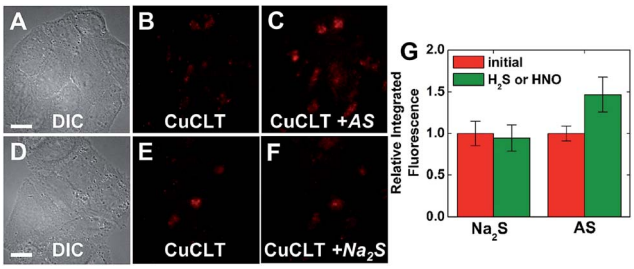

Fig. 7 Fluorescence microscopy images of live HeLa cells incubated with 4 μM CuCLT at 37 °C for 15 min in phosphate buffer saline (PBS). Top: cells treated with Angeli's salt (AS). (A) Differential interference contrast (DIC) image. CuCLT signal (B) before and (C) 10 min after treatment with 1.5 mM AS on the microscope stage. Bottom: cells treated with Na_2S. (D) DIC image. CuCLT signal (E) before and (F) 10 min after treatment with 1.25 mM Na_2S on the microscope stage. (G) Quantification of the intracellular fluorescence response of CuCLT (mean ± SD, $N = 51$ for Na_2S, $N = 44$ for AS). Scale bar = 15 μm. For full-field images and associated nuclear staining, see Fig. S31.†

In order to probe whether CuCLT can detect HNO formed endogenously in a biological process, we applied the sensor in a multicolor imaging experiment to study the reduction of intracellular *S*-nitrosothiols (RSNO) by ascorbate. In the absence of Cu(I) ions, ascorbate reacts with RSNO to generate the corresponding thiol (RSH) and *O*-nitrosoascorbate, which may then further decay following several pathways, one of them yielding HNO and dehydroascorbic acid (Scheme S6, ESI†).[57,58] The HNO thus produced may further react with additional RSNO moieties to liberate NO and RSH.[58] Intracellular generation of HNO following treatment of endothelial cells with ascorbate was recently demonstrated by a combination of amperometric and fluorescence microscopy methods.[14] On the other hand, *S*-nitrosothiols are converted to the corresponding disulfides in the presence of Cu(I), liberating one equiv. of NO per RSNO unit.[46] Thus, the interplay between HNO and NO

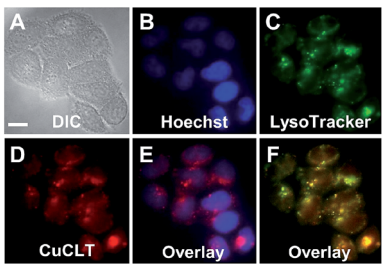

Fig. 8 Co-localization analysis of CuCLT with organelle-specific markers in live HeLa cells incubated with 4 μM CuCLT, 15 μM Hoechst 33258, and 100 nM LysoTracker Green at 37 °C for 15 min in dye- and serum-free DMEM. (A) DIC image. (B) Signal from Hoechst 33258. (C) Signal from LysoTracker Green. (D) Signal from CuCLT. (E) Overlay of Hoechst 33258 and CuCLT. (F) Overlay of LysoTracker Green and CuCLT. Scale bar = 15 μm.

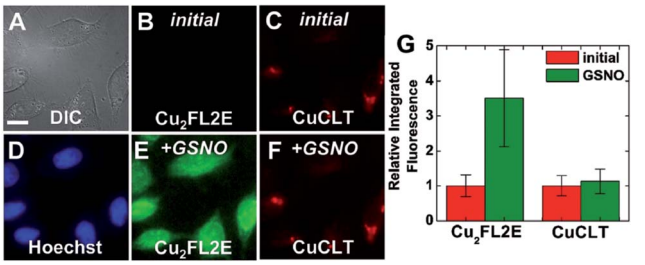

Fig. 9 Multicolor fluorescence microscopy of HeLa cells incubated with 4 μM CuCLT, 15 μM Hoechst 33258, and 2 μM Cu_2FL2E at 37 °C for 15 min in PBS. (A) DIC image. Signal from Cu_2FL2E (B) before and (E) 20 min after treatment with 1.5 mM GSNO on the microscope stage. Signal from CuCLT (C) before and (F) 20 min after treatment with 1.5 mM GSNO. (D) Signal from Hoechst 33258. (G) Quantification of the intracellular fluorescence response of Cu_2FL2E and CuCLT (mean ± SD, $N = 32$). Scale bar = 15 μm.

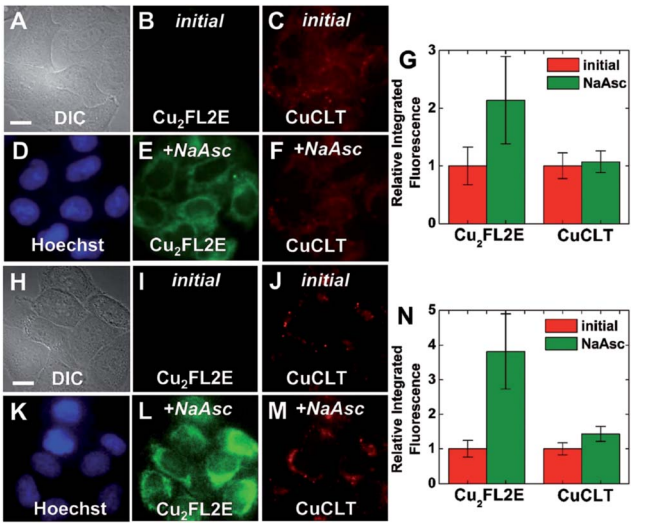

Fig. 10 Multicolor fluorescence microscopy of live HeLa cells incubated with 3 μM CuCLT, 15 μM Hoechst 33258, and 2 μM Cu_2FL2E at 37 °C for 15 min in PBS (A–F) or dye- and serum-free DMEM (H–M). (A–G) Control cells. (A) DIC image. Signal from Cu_2FL2E (B) before and (E) 10 min after treatment with 1.5 mM of sodium ascorbate (NaAsc) on the microscope stage. Signal from CuCLT (C) before and (F) 10 min after treatment with 1.5 mM NaAsc. (D) Signal from Hoechst 33258. (G) Quantification of the intracellular fluorescence response of Cu_2FL2E and CuCLT (mean ± SD, $N = 40$). (H–N) Cells pre-treated with 200 μM DETA NONOate for 20 h at 37 °C in DMEM. (H) DIC image. Signal from Cu_2FL2E (I) before and (L) 10 min after treatment with 1.5 mM of NaAsc. Signal from CuCLT (J) before and (M) 10 min after treatment with 1.5 mM NaAsc. (K) Signal from Hoechst 33258. (N) Quantification of the intracellular fluorescence response of Cu_2FL2E and CuCLT (mean ± SD, $N = 36$). Scale bar = 15 μm.

generated upon cellular stimulation with ascorbate becomes an event that can be visualized with an adequate pair of fluorescent sensors selective for the two analytes. We therefore employed CuCLT and Cu_2FL2E to detect HNO and NO, respectively, in live cells under normal (control) and RSNO-enriched conditions (Fig. 10). The intracellular RSNO content was increased by treatment of the cells with the NO donor DETA NONOate.

Addition of 1.5 mM sodium ascorbate to control cells increased only the intracellular green fluorescence of the NO-selective Cu_2FL2E probe by ~2.1-fold (Fig. 10A–G), whereas addition of the same amount of ascorbate to cells in which intracellular RSNO levels were increased with DETA NONOate enhanced the fluorescence of both Cu_2FL2E and CuCLT by ~3.8-fold and ~1.4-fold, respectively (Fig. 10H–N). Notably, the average value of the intracellular turn-on achieved for CuCLT in DETA NONOate-treated cells upon stimulation with ascorbate matched the positive control for HNO in cells treated with Angeli's salt (Fig. 7G). At the same time, the increase in intracellular RSNO levels and subsequent generation of NO was reflected in the doubling of the average fluorescence turn-on of Cu_2FL2E, consistent with the positive control in cells following exogenous addition of GSNO (Fig. 9G). The lack of a fluorescence response from CuCLT in ascorbate-stimulated control cells suggests that the amount of HNO formed under normal RSNO conditions is too low to allow for intracellular detection by the sensor. In a cuvette, excess addition of an equimolar ascorbate–GSNO mixture to CuCLT in aqueous buffer did not produce an increase in fluorescence (Fig. S37A†), consistent with HNO generated by *O*-nitrosoascorbate at pH 7 being instantly consumed by excess GSNO and glutathione (GSH), in accord with previously reported studies.[58] Formation of glutathione in the reaction of ascorbate with GSNO was demonstrated by the large fluorescence turn-on displayed by the thiol-selective probe CuQLT under similar conditions (Fig. S37B†), an increase much greater than when CuQLT was treated with GSNO alone. Excess ascorbate added to aqueous Cu_2FL2E did not elicit a fluorescence response (Fig. S37C†), confirming that its intracellular fluorescence increase arises from reaction with endogenously produced NO. These results demonstrate the utility of CuCLT for intracellular detection of nitroxyl and strongly suggest that HNO can be produced endogenously in the reaction of ascorbate with *S*-nitrosothiols. A definitive proof of this hypothesis would benefit from *in vivo* studies confirming endogenous HNO production by an orthogonal method.

Intracellular detection of thiols with CuQLT. We also evaluated the ability of RSH-selective CuQLT to detect changes in the concentration of intracellular thiols. A strong intracellular fluorescence signal was observed in the red imaging channel following incubation of HeLa cells with 4 μM CuQLT in PBS, consistent with the probe being turned on by endogenous free thiols (Fig. 11B). CuQLT did not appear to preferentially accumulate within a specific organelle. Upon pre-incubating the cells with *N*-methylmaleimide (NMM), a thiol blocker,[59] we observed a ~3-fold reduction in the integrated fluorescence of CuQLT using identical image acquisition parameters (Fig. 11E), consistent with a decrease in the intracellular free thiol content induced by NMM. Addition of exogenous GSNO to any of the two sets of cells did not produce a fluorescence increase of CuQLT, confirming that the probe can selectively detect biological thiols in live cells over RSNO and NO (Fig. 11C and F).

To reverse the intracellular fluorescence of CuQLT, L-cysteine was first added alone to NMM-treated cells, inducing a strong increase in the signal (Fig. S34†). Addition of 1.5 mM Angeli's salt to NMM-treated cells incubated with CuQLT did not

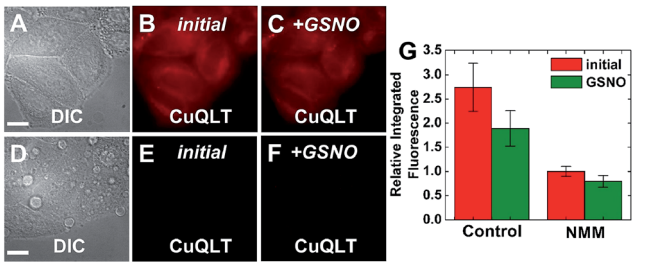

Fig. 11 Fluorescence microscopy images of live HeLa cells incubated with 4 μM CuQLT at 37 °C for 15 min in PBS. Top: control cells. (A) DIC image. CuQLT signal (B) before and (C) 15 min after treatment with 1.5 mM GSNO on the microscope stage. Bottom: cells pre-incubated with 1 mM *N*-methylmaleimide (NMM) in PBS for 30 min at 37 °C. (D) DIC image. CuQLT signal (E) before and (F) 15 min after treatment with 1.5 mM GSNO on the microscope stage. (G) Quantification of the intracellular fluorescence response of CuQLT (mean ± SD, $N = 21$ for control cells, $N = 20$ for NMM-treated cells). Scale bar = 15 μm. For full-field images and associated nuclear staining, see Fig. S33.†

produce a fluorescence increase, but subsequent addition of 3 mM Cys to the same imaging dish elicited a rapid 2-fold enhancement of the signal in the red channel (Fig. S35†). These observations are consistent with the reactivity profile of CuQLT determined in the cuvette (Fig. 5), establishing the selectivity of the probe for thiols in a live environment in the presence of HNO.

Finally, the ability of CuQLT to detect thiols selectively over H_2S in cells was investigated. In contrast to results obtained in the cuvette, adding exogenous Na_2S to NMM-treated cells incubated with CuQLT generated a surprising ~2.4-fold increase in intracellular fluorescence (Fig. 12A–C).

Previous reports proposed exogenous H_2S as a source of endogenous RSH and HSNO, based on its reaction with intracellular RSNO.[12] To further verify this biological pathway, we increased the endogenous RSNO content of the cells by treatment with DETA NONOate and depleted the free thiols with

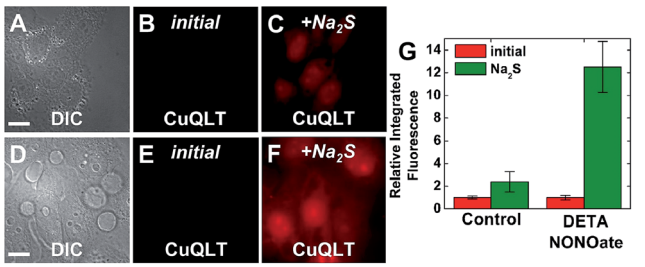

Fig. 12 Fluorescence microscopy images of live HeLa cells incubated with 4 μM CuQLT at 37 °C for 15 min in PBS. Top: control cells. (A) DIC image. CuQLT signal (B) before and (C) 15 min after treatment with 1.25 mM Na_2S on the microscope stage. Bottom: cells pre-treated with 200 μM DETA NONOate for 20 h at 37 °C in DMEM. (D) DIC image. CuQLT signal (E) before and (F) 15 min after treatment with 1.25 mM Na_2S on the microscope stage. Both sets of cells were pre-incubated with 1 mM NMM in PBS for 30 min at 37 °C. (G) Quantification of the intracellular fluorescence response of CuQLT (mean ± SD, $N = 52$ for control cells, $N = 34$ for DETA NONOate-treated cells). Scale bar = 15 μm. For full-field images and associated nuclear staining, see Fig. S36.†

NMM. Addition of Na_2S to these cells brought about a dramatic ~12-fold increase in the integrated CuQLT fluorescence (Fig. 12D–F), an outcome consistent with the intracellular release of a significantly higher amount of thiols. Control experiments in the cuvette confirmed the production of glutathione through the strong increase in the fluorescence of CuQLT upon treatment with an equimolar mixture of Na_2S and GSNO (Fig. S37B†). CuQLT is therefore able to selectively detect RSH in cells and distinguish distinct concentrations of thiols endogenously produced in a biological process.

Conclusions

We established a biocompatible solid-phase approach to separate the fluorescent reporter and binding unit of small-molecule metal-based sensors and tested its modularity by producing three conjugates with a lysine backbone. The first two, functionalized with a yellow-emitting tetramethyl-rhodamine fluorophore, contain an [N_4] (cyclam) and an [N_2O] (quinoline-phenolate) metal-binding site, respectively, while the third retains the [N_2O] motif along with a green-emitting dichlorofluorescein moiety. The active, metal-bound forms of the probes, termed CuCLT, CuQLT, and CuQLF, operate by modulating the oxidation state of a ligated Cu(II) ion. We demonstrated the selectivity of (i) CuCLT for sensing HNO and (ii) CuQLT and CuQLF for sensing biological thiols. The mechanism responsible for the observed reactivity in each case was investigated by spectroscopic (fluorescence, EPR, and NMR) and voltammetric methods. The experimental evidence collected supports a mechanism involving reduction of Cu(II) in CuCLT by HNO followed by a fast reoxidation with retention of the metal in the cyclam binding site, whereas cysteine reduces Cu(II) in CuQLT with attendant expulsion of the Cu(I) species. CuCLT and CuQLT are readily cell permeable and retain their analyte selectivity intracellularly, even in the presence of potentially interfering species such as nitric oxide, nitrosothiols, and hydrogen sulfide. We further employed CuCLT and CuQLT to distinguish between different levels of intracellular HNO and thiols generated upon stimulation of live HeLa cells with ascorbate and sulfide anions, respectively. The successful application of the lysine-based sensors to gain insight into proposed biosynthetic pathways validates the utility of our method and envisions an extension of it from a simple lysine to a peptide backbone. Solid-phase techniques, offering the possibility of altering the light-emitting and metal-binding moieties, provide a tool for expedient production of a library of analogues with minimal synthetic and purification work. Future probes, enacting both predicted and new chemistry, should allow simultaneous and selective multicolor visualization of a variety of species present in live cells, advancing our understanding of their biology.

Acknowledgements

This work was supported by the National Science Foundation under grant CHE-1265770. Spectroscopic instrumentation in the MIT DCIF is maintained with funding from NIH grant

1S10RR13886-01. We thank Dr. Jacob Goldberg for providing a sample of 5-CO_2H-FL. Dr. Timothy Johnstone is gratefully acknowledged for assistance with cyclic voltammetry studies.

Notes and references

1 R. F. Furchgott and J. V. Zawadzki, *Nature*, 1980, **288**, 373–376.
2 M. D. Pluth, E. Tomat and S. J. Lippard, *Annu. Rev. Biochem.*, 2011, **80**, 333–355.
3 V. Calabrese, C. Mancuso, M. Calvani, E. Rizzarelli, D. A. Butterfield and A. M. G. Stella, *Nat. Rev. Neurosci.*, 2007, **8**, 766–775.
4 A. Carreau, C. Kieda and C. Grillon, *Exp. Cell Res.*, 2011, **317**, 29–41.
5 J. J. Turchi, *Proc. Natl. Acad. Sci. U. S. A.*, 2006, **103**, 4337–4338.
6 J. M. Fukuto, A. S. Dutton and K. N. Houk, *ChemBioChem*, 2005, **6**, 612–619.
7 J. M. Fukuto, C. H. Switzer, K. M. Miranda and D. A. Wink, *Annu. Rev. Pharmacol. Toxicol.*, 2005, **45**, 335–355.
8 M. E. Murphy and H. Sies, *Proc. Natl. Acad. Sci. U. S. A.*, 1991, **88**, 10860–10864.
9 N. Sakai, S. Kaufman and S. Milstien, *Mol. Pharmacol.*, 1993, **43**, 6–10.
10 M. A. Sharpe and C. E. Cooper, *Biochem. J.*, 1998, **332**, 9–19.
11 S. Adak, Q. Wang and D. J. Stuehr, *J. Biol. Chem.*, 2000, **275**, 33554–33561.
12 M. R. Filipovic, J. L. Miljkovic, T. Nauser, M. Royzen, K. Klos, T. Shubina, W. H. Koppenol, S. J. Lippard and I. Ivanovic-Burmazovic, *J. Am. Chem. Soc.*, 2012, **134**, 12016–12027.
13 J. L. Miljkovic, I. Kenkel, I. Ivanovic-Burmazovic and M. R. Filipovic, *Angew. Chem., Int. Ed.*, 2013, **52**, 12061–12064.
14 S. A. Suarez, N. I. Neuman, M. Muñoz, L. Álvarez, D. E. Bikiel, C. D. Brondino, I. Ivanović-Burmazović, J. L. Miljkovic, M. R. Filipovic, M. A. Martí and F. Doctorovich, *J. Am. Chem. Soc.*, 2015, **137**, 4720–4727.
15 M. L. Bullen, A. A. Miller, K. L. Andrews, J. C. Irvine, R. H. Ritchie, C. G. Sobey and B. K. Kemp-Harper, *Antioxid. Redox Signaling*, 2011, **14**, 1675–1686.
16 N. Paolocci, W. F. Saavedra, K. M. Miranda, C. Martignani, T. Isoda, J. M. Hare, M. G. Espey, J. M. Fukuto, M. Feelisch, D. A. Wink and D. A. Kass, *Proc. Natl. Acad. Sci. U. S. A.*, 2001, **98**, 10463–10468.
17 C. U. Choe, J. Lewerenz, C. Gerloff, T. Magnus and S. Donzelli, *Antioxid. Redox Signaling*, 2011, **14**, 1699–1711.
18 L. E. McQuade and S. J. Lippard, *Curr. Opin. Chem. Biol.*, 2010, **14**, 43–49.
19 *The Molecular Probes Handbook*, ed. I. Johnson and M. T. Z. Spence, Life Technologies, 2010.
20 M. H. Lim, B. A. Wong, W. H. Pitcock, Jr., D. Mokshagundam, M.-H. Baik and S. J. Lippard, *J. Am. Chem. Soc.*, 2006, **128**, 14364–14373.
21 M. H. Lim, D. Xu and S. J. Lippard, *Nat. Chem. Biol.*, 2006, **2**, 375–380.
22 L. E. McQuade and S. J. Lippard, *Inorg. Chem.*, 2010, **49**, 7464–7471.
23 L. E. McQuade, J. Ma, G. Lowe, A. Ghatpande, A. Gelperin and S. J. Lippard, *Proc. Natl. Acad. Sci. U. S. A.*, 2010, **107**, 8525–8530.
24 M. D. Pluth, L. E. McQuade and S. J. Lippard, *Org. Lett.*, 2010, **12**, 2318–2321.
25 M. D. Pluth, M. R. Chan, L. E. McQuade and S. J. Lippard, *Inorg. Chem.*, 2011, **50**, 9385–9392.
26 U. P. Apfel, D. Buccella, J. J. Wilson and S. J. Lippard, *Inorg. Chem.*, 2013, **52**, 3285–3294.
27 A. T. Wrobel, T. C. Johnstone, A. D. Liang, S. J. Lippard and P. Rivera-Fuentes, *J. Am. Chem. Soc.*, 2014, **136**, 4697–4705.
28 H. Wang, G. Zhou and X. Chen, *Sens. Actuators, B*, 2013, **176**, 698–703.
29 L. E. McQuade, M. D. Pluth and S. J. Lippard, *Inorg. Chem.*, 2010, **49**, 8025–8033.
30 J. Rosenthal and S. J. Lippard, *J. Am. Chem. Soc.*, 2010, **132**, 5536–5537.
31 M. D. Bartberger, W. Liu, E. Ford, K. M. Miranda, C. Switzer, J. M. Fukuto, P. J. Farmer, D. A. Wink and K. N. Houk, *Proc. Natl. Acad. Sci. U. S. A.*, 2002, **99**, 10958–10963.
32 R. A. Alberty, *Biophys. Chem.*, 2004, **111**, 115–122.
33 E. A. Ambundo, M. V. Deydier, A. J. Grall, N. Aguera-Vega, L. T. Dressel, T. H. Cooper, M. J. Heeg, L. A. Ochrymowycz and D. B. Rorabacher, *Inorg. Chem.*, 1999, **38**, 4233–4242.
34 K. Sasakura, K. Hanaoka, N. Shibuya, Y. Mikami, Y. Kimura, T. Komatsu, T. Ueno, T. Terai, H. Kimura and T. Nagano, *J. Am. Chem. Soc.*, 2011, **133**, 18003–18005.
35 K. Kawai, N. Ieda, K. Aizawa, T. Suzuki, N. Miyata and H. Nakagawa, *J. Am. Chem. Soc.*, 2013, **135**, 12690–12696.
36 Z. R. Miao, J. A. Reisz, S. M. Mitroka, J. Pan, M. Xian and S. B. King, *Bioorg. Med. Chem. Lett.*, 2015, **25**, 16–19.
37 M. G. Choi, S. Cha, H. Lee, H. L. Jeon and S. K. Chang, *Chem. Commun.*, 2009, 7390–7392.
38 X. Chen, Y. Zhou, X. Peng and J. Yoon, *Chem. Soc. Rev.*, 2010, **39**, 2120–2135.
39 H. Peng, W. Chen, Y. Cheng, L. Hakuna, R. Strongin and B. Wang, *Sensors*, 2012, **12**, 15907–15946.
40 H. S. Jung, X. Chen, J. S. Kim and J. Yoon, *Chem. Soc. Rev.*, 2013, **42**, 6019–6031.
41 M. V. Kvach, I. A. Stepanova, I. A. Prokhorenko, A. P. Stupak, D. A. Bolibrukh, V. A. Korshun and V. V. Shmanai, *Bioconjugate Chem.*, 2009, **20**, 1673–1682.
42 E. S. Rector, K. S. Tse, A. H. Sehon and R. J. Schwenk, *J. Immunol. Methods*, 1978, **24**, 321–336.
43 C. C. Woodroofe, R. Masalha, K. R. Barnes, C. J. Frederickson and S. J. Lippard, *Chem. Biol.*, 2004, **11**, 1659–1666.
44 S. B. King and H. T. Nagasawa, *Methods Enzymol.*, 1999, **301**, 211–220.
45 K. M. Miranda, A. S. Dutton, L. A. Ridnour, C. A. Foreman, E. Ford, N. Paolocci, T. Katori, C. G. Tocchetti, D. Mancardi, D. D. Thomas, M. G. Espey, K. N. Houk, J. M. Fukuto and D. A. Wink, *J. Am. Chem. Soc.*, 2005, **127**, 722–731.
46 R. J. Singh, N. Hogg, J. Joseph and B. Kalyanaraman, *J. Biol. Chem.*, 1996, **271**, 18596–18603.

47 M. Sauer, K. T. Han, R. Muller, S. Nord, A. Schulz, S. Seeger, J. Wolfrum, J. Arden-Jacob, G. Deltau, N. J. Marx, C. Zander and K. H. Drexhage, *J. Fluoresc.*, 1995, **5**, 247–261.
48 V. Shafirovich and S. V. Lymar, *Proc. Natl. Acad. Sci. U. S. A.*, 2002, **99**, 7340–7345.
49 W. Flores-Santana, D. J. Salmon, S. Donzelli, C. H. Switzer, D. Basudhar, L. Ridnour, R. Cheng, S. A. Glynn, N. Paolocci, J. M. Fukuto, K. M. Miranda and D. A. Wink, *Antioxid. Redox Signaling*, 2011, **14**, 1659–1674.
50 I. M. Wasser, S. de Vries, P. Moenne-Loccoz, I. Schroder and K. D. Karlin, *Chem. Rev.*, 2002, **102**, 1201–1234.
51 S. Kim, M. A. Siegler and K. D. Karlin, *Chem. Commun.*, 2014, **50**, 2844–2846.
52 A. Rigo, A. Corazza, M. L. di Paolo, M. Rossetto, R. Ugolini and M. Scarpa, *J. Inorg. Biochem.*, 2004, **98**, 1495–1501.
53 X. F. Yang, P. Liu, L. Wang and M. Zhao, *J. Fluoresc.*, 2008, **18**, 453–459.
54 H. S. Jung, J. H. Han, Y. Habata, C. Kang and J. S. Kim, *Chem. Commun.*, 2011, **47**, 5142–5144.
55 V. Zinchuk, Y. Wu and O. Grossenbacher-Zinchuk, *Sci. Rep.*, 2013, **3**, 1365.
56 A. P. French, S. Mills, R. Swarup, M. J. Bennett and T. P. Pridmore, *Nat. Protoc.*, 2008, **3**, 619–628.
57 A. Kytzia, H. G. Korth, R. Sustmann, H. de Groot and M. Kirsch, *Chem.–Eur. J.*, 2006, **12**, 8786–8797.
58 M. Kirsch, A. M. Buscher, S. Aker, R. Schulz and H. de Groot, *Org. Biomol. Chem.*, 2009, **7**, 1954–1962.
59 J. Yin, Y. Kwon, D. Kim, D. Lee, G. Kim, Y. Hu, J. H. Ryu and J. Yoon, *J. Am. Chem. Soc.*, 2014, **136**, 5351–5358.